Numerical Studies of Transient Opposed-Flow Flames using Adaptive Time Integration

Hong Geun Im*
(Sandia National Laboratories Livermore, USA)

Numerical simulations of unsteady opposed-flow flames are performed using an adaptive time integration method designed for differential-algebraic systems. The compressibility effect is considered in deriving the system of equations, such that the numerical difficulties associated with a high-index system are alleviated. The numerical method is implemented for systems with detailed chemical mechanisms and transport properties by utilizing the Chemkin software. Two test simulations are performeds hydrogen/air diffusion flames with an oscillatory strain rate and transient ignition of methane against heated air. Both results show that the rapid transient behavior is successfully captured by the numerical method.

Key Words : Unsteady Flames, Adaptive Time Integration

Nomenclature

A : Amplitude of the nozzle exit velocity oscillation
b_1, b_2 : Grid refinement parameter
C : Grid refinement parameter
c_p : Mixture specific heat
D_{kj} : Multicomponent diffusion coefficient
D_{km} : Binary diffusion coefficient
$\mathcal{D}_{jk}$: Mixture-averaged diffusion coefficient
D_k^T : Thermal diffusion coefficient
f : Frequency of the nozzle exit velocity oscillation
h_k : Enthalpy of formation of the k-th species
J : Total number of grid points
K : Total number of species
L : Nozzle separation
Ma : Mach number
P : Total pressure
p_0 : Thermodynamic pressure
p : Hydrodynamic pressure
r : Radial coordinate
T : Temperature
t : Time
u : Axial velocity
u_c : Characteristic velocity
V : v/r
v : Radial velocity
X_k : Mole fraction of the k-th species
x : Axial coordinate
$\bar{W}$: Average molecular weight
W_k : Molecular weight of the k-th species
Y_k : Mass fraction of the k-th species
Z : Elemental mass fraction

Greek Symbols

Δx : Grid spacing
ρ : Density
Λ : Pressure eigenvalue $((1/r)(\partial p/\partial r))$
λ : Mixture thermal conductivity
μ : Mixture molecular viscosity
η : Transformed coordinate defined in Eq. (27)
χ : Scalar dissipation rate
ϕ : Substitute function defined as $d\phi/dt = \Lambda(t)$
σ : Numerical damping factor
ξ : Mixture fraction defined in Eq. (30)
ω_k : Molar reaction rate for the k-th species

Subscripts

F : Fuel side boundary $(x=0)$

* Corresponding Author, **E-mail** : hgim@umich.edu
TEL : +1-925-294-3131 ; **FAX** : +1-925-294-2595
Combustion Research Facility, MS9051 Sandia National Laboratories Livermore, CA 94551-0969, USA. (Manuscript Received May 28, 1999 ; Revised October 11, 1999)

J : Grid point at $x=L$
O : Oxidizer side boundary ($x=L$)

1. Introduction

The opposed-flow geometry serves as a convenient configuration to study the effects of flow straining on the behavior of laminar flames, and provides useful fundamental characteristics that represent turbulent combustion in the laminar flamelet regime. By adopting a similarity coordinate, the mathematical system can be reduced into a set of one-dimensional equations, hence facilitating computational and analytic studies. Furthermore, an experimental apparatus can be easily set up, allowing for direct quantitative comparison between model predictions and measured data. Therefore, the opposed-flow flames have been extensively studied as a canonical system for understanding flame structures (Lee *et al.*, 1995) and validating various chemical kinetics and transport models.

As understanding of steady laminar flames has improved, the effects of flow unsteadiness has recently attracted more attention for its relevance in turbulent combustion which exhibits a wide spectrum of length and time scales. However, robust numerical integration of fast transient combustion processes with spatial/temporal stiffness is difficult due to the associated compressible gas dynamic behavior. From a mathematical standpoint, the standard opposed-flow formulation with a constant pressure approximation results in a system of high-index differential-algebraic equations (DAE's). Thus, time integration with rigorous error and time-step control can be numerically unstable during the periods of rapid change in the solution (Brenan *et al.*, 1996 ; Ascher and Petzold, 1998). Moreover, for problems with rapid transients such as ignition, adaptive time-step control is needed for efficient time-integration without sacrificing the overall accuracy of the solution.

In this study, a new unsteady opposed-flow formulation is developed and tested under various transient problems. The code is based on the steady counterpart, OPPDIF (Lutz *et al.*, 1996), replacing Twopnt (Grcar, 1992), the steady Newton solver, with DASSL (Petzold, 1982), a solution package for a DAE system. Chemkin (Kee *et al.*, 1991) and Transport (Kee *et al.*, 1986) interfaces are used to determine chemical reaction rates and transport properties. DASSL incorporates a variable-order, variable-step backward differentiation formula (BDF) to solve general index-1 DAE's, thereby facilitating a robust time integration of stiff transient problems. In addition to this, the mathematical formulation is also modified to alleviate numerical difficulty associated with the high-index nature of the DAE system.

In the next section, the incompressible flow formulation is first described following the formulations used in the steady opposed-flow problems, and the numerical difficulty of the high-index system is discussed. A modified, compressible formulation is then derived by partially relaxing the boundary layer approximation. Methods for index reduction are also discussed. Subsequently, the capability of the code is demonstrated by the results of oscillatory diffusion flames and transient ignition problems.

2. Incompressible-Flow Formulation: High-Index DAE's

Figure 1 shows a schematic of the system configuration. Two opposing axisymmetric nozzles are separated by a distance of L. Fuel and oxidizer are supplied at $x=0$ and $x=L$, respectively, thereby forming a diffusion flame in the vicinity of the stagnation plane. To capture the unsteady flame response, the grid is refined so that the fine grid structure is mapped over the range of the reaction zone movement.

The governing equations for the unsteady opposed-flow geometry follows the formulation by Kee et al. (1988) derived for the finite-distance opposing nozzles. The earlier conventional potential-flow formulation (Schlichting, 1979) has only one parameter the strain rate. In contrast, the present formulation introduces an extra degree of freedom such that the velocities at both nozzle exits are given and the strain rate is

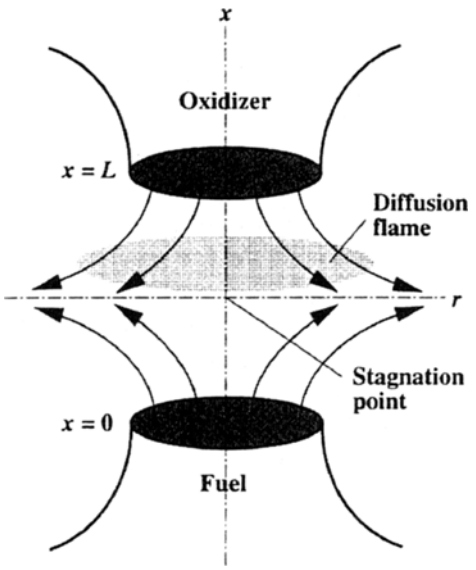

Fig. 1 Schematic of the system configuration

computed as a solution.

Assuming similarity near the centerline, the axial velocity, radial velocity, temperature and species mass fractions are given as functions of time and the axial coordinate only:

$$u=u(t, x),\ v/r=V(t, x),$$
$$T=T(t, x),\ Y_k=Y_k(t, x). \tag{1}$$

For a system whose characteristic velocity scale is much smaller than the speed of sound, *i. e.* $Ma=u_c/a\ll 1$, the pressure, P, can be decomposed into the thermodynamic (p_0) and hydrodynamic (p) components by an asymptotic expansion in Ma. Furthermore, the boundary layer approximation leads to $\partial P/\partial x=0$, such that:

$$P=p_0(t)+p(t, r)+o(Ma^2). \tag{2}$$

where $p/p_0=o(Ma^2)$. Using the boundary layer approximation in the axial direction, the conservation equations become:

- Mass continuity:

$$\frac{\partial \rho}{\partial t}+\frac{\partial}{\partial x}(\rho u)+2\rho V=0, \tag{3}$$

- Radial momentum:

$$\rho\frac{\partial V}{\partial t}+\rho u\frac{\partial V}{\partial x}+\rho V^2-\frac{\partial}{\partial x}\left(\mu\frac{\partial V}{\partial x}\right)+\Lambda=0, \tag{4}$$

- Energy conservation:

$$\rho c_p\frac{\partial T}{\partial t}+\rho c_p u\frac{\partial T}{\partial x}-\frac{\partial}{\partial x}\left(\lambda\frac{\partial T}{\partial x}\right)-\frac{\partial p_0}{\partial t}$$
$$+\rho\left(\sum_k c_p Y_k V_k\right)\frac{\partial T}{\partial x}+\sum_k h_k W_k\omega_k=0, \tag{5}$$

- Species conservation:

$$\rho\frac{\partial Y_k}{\partial t}+\rho u\frac{\partial Y_k}{\partial x}+\frac{\partial}{\partial x}(\rho Y_k V_k)-W_k\omega_k$$
$$=0,\ k=1, \cdots, K, \tag{6}$$

where

$$\Lambda(t)=\frac{1}{r}\frac{\partial p}{\partial r} \tag{7}$$

is the eigenvalue of the system to be solved with other dependent variables. To maintain the banded structure of the iteration matrix, a trivial equation

$$\frac{\partial \Lambda}{\partial x}=0 \tag{8}$$

is added.

Other constitutive relations include the equation of state

$$\rho=P\bar{W}/RT \tag{9}$$

and the diffusion velocity, V_k, is given by either the multicomponent formulation

$$V_k=\frac{1}{X_k\bar{W}}\sum_{j=1}^{K}W_j D_{kj}\frac{dX_j}{dx}-\frac{D_k^T}{\rho Y_k}\frac{1}{T}\frac{dT}{dx}, \tag{10}$$

or the mixture-averaged formulation

$$V_k=-\frac{1}{X_k}D_{km}\frac{dX_k}{dx}-\frac{D_k^T}{\rho Y_k}\frac{1}{T}\frac{dT}{dx}$$
$$D_{km}=\frac{1-Y_k}{\sum_{j\neq k}^{K}X_j/\mathcal{D}_{jk}}, \tag{11}$$

where D_{kj}, D_{km}, $\mathcal{D}_{jk}$ and D_k^T are the multicomponent, binary, mixture-averaged, and thermal diffusion coefficients, respectively. Also, X_i is the mole fraction of species i, c_k is the specific heat of the mixture. μ is the thermal conductivity of the mixture, h_k is the enthalpy of formation. W_k is the molecular weight of species k, and $\bar{W}$ is the mixture-averaged molecular weight.

The above system of equations are subject to the following boundary conditions:

$$\begin{aligned}&x=0: u=u_F(t),\quad V=V_F(t),\\ &T=T_F(t),\quad Y_k=(Y_k)_F(t),\\ &x=L: u=u_O(t),\quad V=V_O(t),\\ &T=T_O(t),\quad Y_k=(Y_k)_O(t),\end{aligned} \tag{12}$$

where subscripts F and O denote the fuel and

oxidizer streams, respectively. Note that, in the present formulation of finite nozzle spacing, both axial and radial velocities can be independently prescribed at the boundary, although $V=0$ is the most common choice for practical cases. Obviously, when the boundary temperatures are varied, density and pressure must be adjusted to satisfy the equation of state. Similarly, species mass fraction variation must be done while satisfying the equation of state and mass conservation, $\sum Y_k=1$. To avoid excessive complexity in prescribing the boundary conditions, the present code is set up such that only one variable, *i. e.* temperature or one specific species, can be varied in time at each boundary.

From a mathematical standpoint, Eqs. (3)-(6) and (8), after a spatial discretization, are viewed as a system of differential-algebraic equations with a solution vector $[u_j, V_j, T_j, (Y_k)_j, \Lambda_j]^T$, where the subscript j denotes grid points that range from 1 to J. In this case, u_j and Λ_j (and the boundary nodes for V, T and Y_k) constitute the algebraic variables due to the absence of $\partial u/\partial t$ and $\partial \Lambda/\partial t$ terms in the corresponding equations. These dependent variables can be grouped into three different kinds of solution vectors as follows:

$$\begin{aligned}\mathbf{x}&=[V_2, T_2, (Y_k)_2, \cdots, V_{J-1}, T_{J-1}, (Y_k)_{J-1}]^T,\\ \mathbf{y}&=[u_1, \cdots, u_J, \Lambda_1, \cdots, \Lambda_{J-1}, V_1, V_J, T_1, T_J,\\ &\quad (Y_k)_1, (Y_k)_J]^T,\\ \mathbf{z}&=[\Lambda_J].\end{aligned} \tag{13}$$

Then the DAE system of the present problem can be written as:

$$\begin{aligned}\frac{d\mathbf{x}}{dt}&=\mathbf{f}(\mathbf{x}, \mathbf{y}, \mathbf{z})\\ 0&=\mathbf{g}(\mathbf{x}, \mathbf{y})\\ 0&=\mathbf{h}(\mathbf{y}).\end{aligned} \tag{14}$$

Equation (14) reveals the distinction between the two algebraic variables $\mathbf{y}$ and $\mathbf{z}$. In this problem, the Jacobian $\mathbf{g}_y$ is nonsingular and all the entries in $\mathbf{y}$ are index-1 variables (Brenan *et al.*, 1996 ; Ascher and Petzold, 1998). On the other hand, the variable $\mathbf{z}$, which represents Λ_J, has an index higher than two because the Jacobian $\mathbf{h}_x\mathbf{f}_z$ becomes singular. This is due to the fact that no explicit equation can be found to solve for the eigenvalue, $\Lambda(t)$; hence a boundary condition such as $u=u_0(t)$ is used for the algebraic equation $0=\mathbf{h}(\mathbf{y})$. Consequently, numerical integration of the high-index system, Eqs. (3)-(6) and (8), encounters difficulties for stiff problems since DASSL is an index-1 solver. These difficulties are alleviated by modifying the formulation as described in the next section.

3. Compressible-Flow Formulation with Index Reduction

Mathematically, the system has a higher index because Λ and u are not closely coupled due to the boundary layer approximation. Physically, the stiffness problem can be interpreted as fast transients associated with rapid gas-dynamic response, which cannot be properly captured by completely eliminating the hydrodynamic pressure from the system. That is, some spatial pressure distribution must be considered in addition to the indirect pressure effect represented by the eigenvalue, Λ. A more direct coupling between Λ and u can be achieved by relaxing the boundary layer approximation and re-introducing the pressure component. Similarity assumption is still needed, however, to retain one-dimensional formulation. Therefore, the pressure expression is modified as:

$$P=p_0(t)+p(t, x)+\frac{1}{2}\Lambda(t)r^2+o(Ma^2) \tag{15}$$

such that p is introduced as an additional dependent variable, where $p/p_0=o(Ma^2)$. The axial momentum equation is also retrieved to solve for the additional variable. By differentiating the equation of state,

$$\frac{\partial \rho}{\partial t}=\frac{\rho}{P}\frac{\partial p}{\partial t}-\frac{\rho}{T}\frac{\partial T}{\partial t}-\rho\bar{W}\sum_k\frac{1}{W_k}\frac{\partial Y_k}{\partial t}, \tag{16}$$

and substituting the $\partial\rho/\partial t$ term in the continuity Eq. (3) of the incompressible-flow formulation, the conservation equations can be rewritten as (Raja *et al.*, 1998):

- Mass continuity:

$$\frac{\rho}{P}\frac{\partial p}{\partial t}-\frac{\rho}{T}\frac{\partial T}{\partial t}-\rho\bar{W}\sum_k\frac{1}{W_k}\frac{\partial Y_k}{\partial t}$$

$$+\frac{\partial}{\partial x}(\rho u)+2\rho V=0, \tag{17}$$

● Axial momentum:

$$\rho\frac{\partial u}{\partial t}+\rho u\frac{\partial u}{\partial x}+\frac{\partial p}{\partial x}-2\mu\frac{\partial V}{\partial x}-\frac{4}{3}\frac{\partial}{\partial x}\left(\mu\frac{\partial u}{\partial x}\right)+\frac{4}{3}\frac{\partial}{\partial x}(\mu V)=0, \tag{18}$$

● Radial momentum:

$$\rho\frac{\partial V}{\partial t}+\rho u\frac{\partial V}{\partial x}+\rho V^2-\frac{\partial}{\partial x}\left(\mu\frac{\partial V}{\partial x}\right)+\Lambda=0, \tag{19}$$

● Energy conservation:

$$\rho c_p\frac{\partial T}{\partial t}+\rho c_p u\frac{\partial T}{\partial x}-\frac{\partial}{\partial x}\left(\lambda\frac{\partial T}{\partial x}\right)-\frac{\partial p_0}{\partial t}-u\frac{\partial p}{\partial x}+\rho\left(\sum_k c_p Y_k V_k\right)\frac{\partial T}{\partial x}+\sum_k h_k W_k\omega_k=0, \tag{20}$$

● Species conservation:

$$\rho\frac{\partial Y_k}{\partial t}+\rho u\frac{\partial Y_k}{\partial x}+\frac{\partial}{\partial x}(\rho Y_k V_k)-W_k\omega_k=0, \quad k=1, \cdots, K. \tag{21}$$

In this new formulation, u at the interior nodes ($j=2, \cdots, J-1$) are changed to differential variables. Furthermore, the boundary condition $u=u_o$ is now used in the J-th node of the axial momentum equation, and the high-index algebraic equation for Λ is replaced by another condition. Since the pressure, p, is introduced as a new dependent variable, a pressure boundary condition is also required. While there is no unique way to identify a physical boundary condition, we adopt the Bernoulli equation at the nozzle exit at $x=L$,

$$p_J+\frac{1}{2}\rho_J u_J^2=\text{constant}. \tag{22}$$

Note that, if Eq. (22) is used as the algebraic equation for Λ, differentiating it twice yields a differential equation form for Λ, recognizing the relation between Λ and p via Eqs. (17) and (19). Therefore, the index of Λ is reduced to 2. Further index reduction can be achieved by a simple substitution

$$\frac{d\phi}{dt}=\Lambda(t) \tag{23}$$

with any arbitrary initial condition for ϕ, since only $d\phi/dt$ appears in the system of equations.

In summary, Eqs. (17)-(21) have become an index-1 system through the following procedure. The algebraic Equation (22) is differentiated once with respect to t to yield an equation for $\partial V/\partial t$, which is further substituted by $d\phi/dt$ via the radial momentum equation.

4. Numerical Methods

Numerical integration of the DAE system, Eqs. (17)-(21), is performed using DASSL. Since DASSL requires that the initial condition must satisfy all the equations in the DAE system, a fully converged steady solution field is used as the initial condition. Due to the modified grid structure as described in the following, a modified version of Oppdif is used to obtain the initial condition.

To fit the modified formulation, a staggered grid system is used as shown in Fig. 2. The grid stencil and boundary conditions for individual dependent variables are shown in separate columns. All dependent variables are represented at the control-volume center nodes, except the axial velocity which is represented at the control-volume faces. The grid indices are shown on the left and the face indices on the right. The right-facing protuberance on the stencils indicates where the time derivative is evaluated. For the pressure-eigenvalue equation there is no time derivative, which is indicated by an unfilled protuberance.

Spatial discretization uses finite differencing for a non-uniform grid system. For the species, energy, and radial momentum equations, a second-order central differencing is used for the diffusive terms, and either first-order upwind or second-order central differencing is used for the convective terms. The continuity equation is spatially first order, using a central difference formulation with u at the cell surfaces. The axial momentum equation is second order in velocity and first order in pressure, utilizing the staggered-grid system.

Because the central differencing on the continuity equation is only neutrally stable, an artificial damping term is introduced to maintain numerical stability. A first-order damping term of the form $\sigma(\Delta x)(\partial^2 p/\partial x^2)$ is added in the continuity

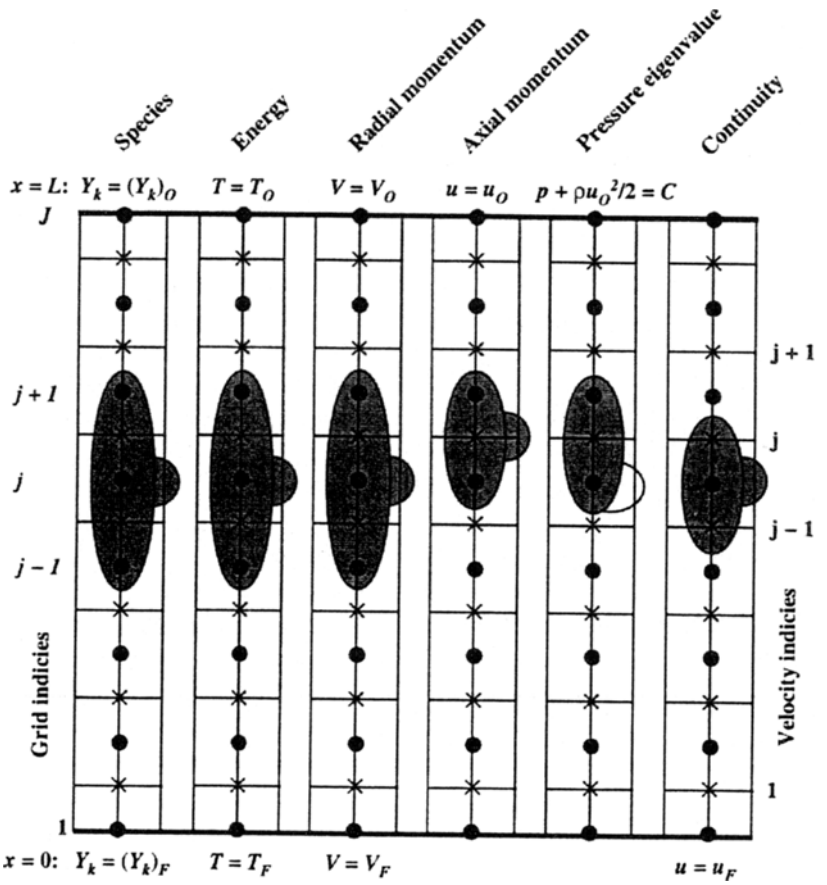

Fig. 2 Schematic of the grid configuration using a finite-volume, staggered-grid spatial-difference stencil

equation, where a sufficiently small value for σ is used to ensure that the solution is not affected. From our experience, $\sigma \approx 10^{-3}$ appears to be acceptable without noticeably affecting the final solution.

The unsteady calculation requires a fully-converged steady solution as an initial condition. To accommodate the transient response of the reaction zone, an *a priori* grid refinement is needed, as described in the following.

First, a grid redistribution is done with a weighting function. Temperature is typically used as the gauge variable and the grid redistribution uses a transformation from the physical coordinate x to a new coordinate η,

$$\frac{dx}{d\eta} W(x, T) = C \tag{24}$$

with the weighting function

$$W(x, T) = 1 + b_1 \left| \frac{dT}{dx} \right| + b_2 \left| \frac{d^2 T}{dx^2} \right|. \tag{25}$$

The constant C is defined by the integration over the entire domain :

$$C = \frac{1}{N-1} \int_0^L W(x, T)\, dx, \tag{26}$$

where N is the total number of grid points. Integrating over a portion of the domain gives an expression for the locations in the η-coordinate space :

$$\eta = 1 + \frac{1}{C} \int_0^x W(x, T)\, dx. \tag{27}$$

The new grid locations, x, are obtained by interpolation between the computed values of η defined using the old mesh, onto a uniform mesh in the η-space. Since $d\eta$ is constant on this uniform mesh, the solution of Eq. (24) states that

$W(x, T) \cdot x$ is constant, and the new values of x are concentrated where the weighting function is large. The parameters, b_1, b_2 and C are adjusted to produce a desired grid system.

5. Results and Discussion

5.1 Oscillatory hydrogen/air diffusion flames

We first present the results for a hydrogen/air diffusion flame subjected to an oscillatory strain rate. First, a steady diffusion flame is solved for the boundary conditions of $u_F = u_O = 100$ cm/sec, $T_F = T_O = 300$K. The species boundary conditions are $X_{H_2} = 0.5$, $X_{N_2} = 0.5$ at $x = 0$ and $X_{O_2} = 0.21$, $X_{N_2} = 0.79$ at $x = L$. Pressure p_0 is assigned a constant value of 1 atm. The reaction mechanism by Yetter *et al.* (1991) is used. Once the steady condition is obtained, the unsteady solution is computed using the time-dependent boundary condition for the axial velocity :

$$u_F(t) = u_O(t) = 100 \times [1 + A\{1 - \cos(2\pi f t)\}], \quad (28)$$

such that the velocity varies from 100 cm/sec to 100(1+2A) cm/sec, at a frequency of f Hz. In this calculation, $A = 0.1$ and $f = 100$ Hz.

Figure 3 shows the spatial profiles of axial velocity and temperature for the steady diffusion flame used as the initial condition for the unsteady calculation. The refined grid system successfully resolves the solution field with large gradients. Figure 4 further shows the profiles of the mole fraction of minor species.

In combustion problems, the characteristic flow time scale is commonly represented by the scalar dissipation rate, defined as

$$\chi_{st} = 2\frac{\lambda}{\rho c_p}(\partial\xi/\partial x)^2|_{\xi=\xi_{st}}. \quad (29)$$

where the substitute st denotes the stoichiometric condition. The mixture fraction, ξ, is defined as a linear combination of the elemental mass fractions, Z_C, Z_H and Z_O (Bilger, 1988) :

$$\xi = \frac{2Z_C/W_C + 1/2Z_H/W_H + (Z_{O,O} - Z_O)/W_O}{2Z_C/W_C + 1/2Z_{H,F}/W_H + Z_{O,O}/W_O}, \quad (30)$$

where the subscripts F and O respectively denote the fuel and oxidizer streams, and W_C, W_H and W_O are the molecular weights of C, H and O atoms, respectively. Note that $Z_C = 0$ for the hydrogen/air system due to the absence of carbon atoms.

Figure 5 shows the response of the scalar

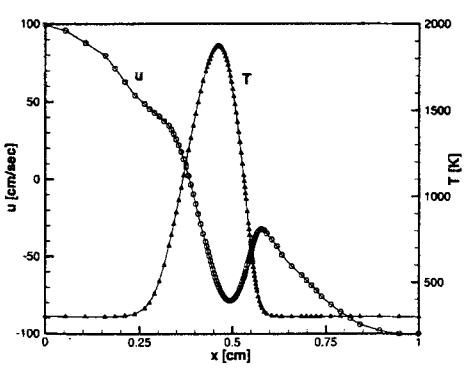

Fig. 3 Axial velocity and temperature profile for the steady hydrogen/air diffusion flame

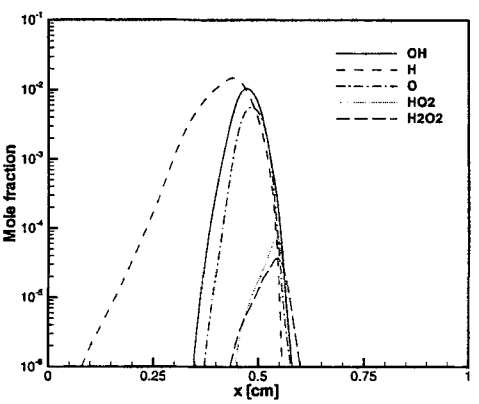

Fig. 4 Profiles of mole fraction of minor species for the steady hydrogen/air diffusion flame

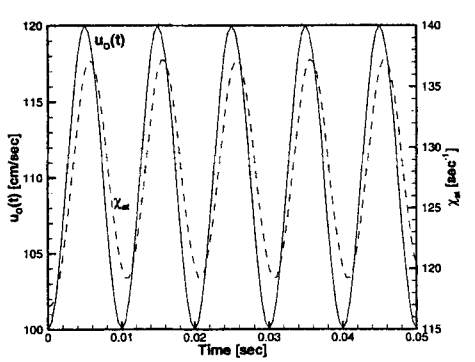

Fig. 5 Imposed axial velocity oscillation and the response of scalar dissipation rate as a function of time for the unsteady hydrogen/air diffusion flame subjected to oscillatory strain rate

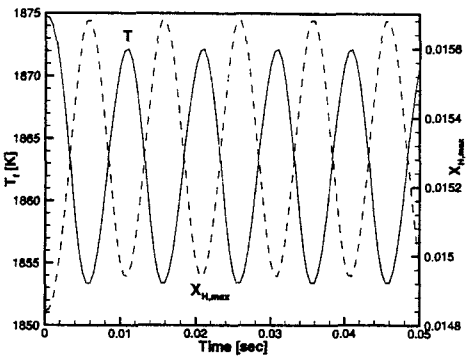

Fig. 6 Unsteady response of the flame temperature and the maximum mole fraction of H atom as a function of time for the unsteady hydrogen/air diffusion flame subjected to oscillatory strain rate

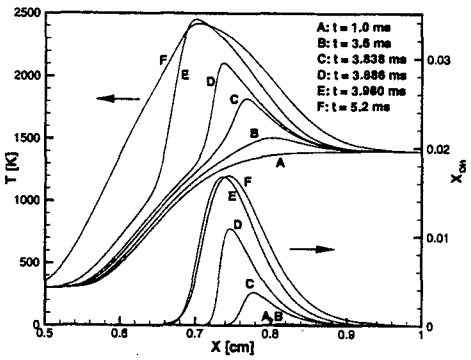

Fig. 7 Evolution of temperature and OH profiles during ignition for $u_0=1$ m/sec or $\chi_{st}=7.06$

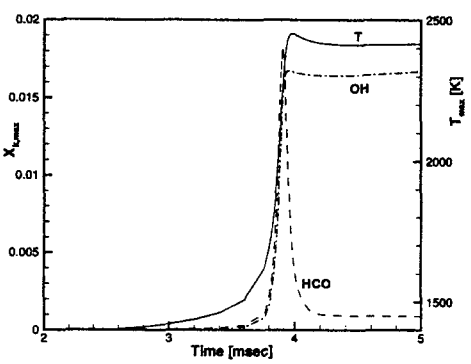

Fig. 8 Transient evolution of the spatial maximum temperature, OH and HCO mole fractions for $u_0=1$ m/sec or $\chi_{st}=7.06$

dissipation rate to the oscillatory nozzle velocity. It is shown that at $f=100$Hz, the scalar dissipation rate shows a small phase delay compared to the imposed velocity fluctuation. The response of maximum flame temperature and maximum H mole fraction is shown in Fig. 6. Comparing with Fig. 5, the maximum temperature decreases and H atom concentration increases for higher scalar dissipation rates, implying an increase in the the degree of incomplete combustion.

5.2 Ignition of methane versus heated air

Next, we consider the ignition problem in a pure methane against hot air under constant pre-ignition strain rates, using GRI v1. 2 (Frenklach *et al.*, 1995) as the chemical mechanism. The nozzle separation is fixed at 1 cm and the pressure is at 1 atm. The fuel-side temperature is held at 300K and the hot-air temperature is at 1400K, which is the main ignition heat source. Under this condition, the steady ignition limit is found to be at $\chi_{st}=17.3s^{-1}$, which occurs at $u_0=u_L=2.2$ m/s, where χ_{st} is the scalar dissipation rate defined in Eq. (29). It has been shown that χ_{st} better represents the flow residence time scale than the strain rate in unsteady flows with fast time scales (Im *et al.*, 1999). For each transient calculation, a steady solution is obtained with identical boundary conditions by suppressing all reaction rates. This solution is then used as the initial condition. The effects of strain rates on ignition are studied by computing solutions for various values of χ_{st} in ignitable states ($\chi_{st}<17.3$).

Figure 7 illustrates a typical evolution of temperature and OH profiles through the ignition event. During a very short period of time (B to E), the ignition kernel develops and propagates into the location at which the diffusion flame is established. The temporal evolution of the spatial maximum values for temperature and a few intermediate species are further shown in Fig. 8. The temporal change of some minor intermediates, such as HCO, exhibits a fast transient response. The adaptive, stiff time integrator employed in this study permits large time steps throughout most of the calculation, while accurately capturing the abrupt transients when necessary.

From Fig. 8, the ignition delay can be defined as the time at which the steep temperature rise occurs. The variation of ignition delay for a range

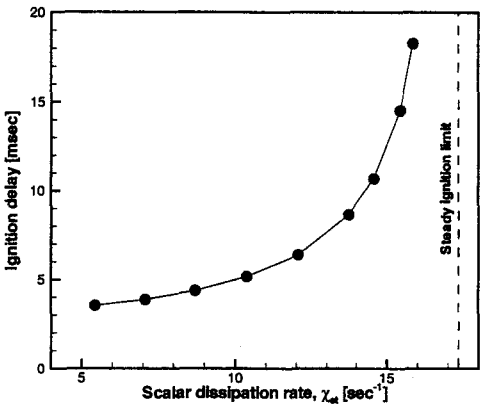

Fig. 9 Ignition delay as a function of the scalar dissipation rate, demonstrating the sensitive response near the steady ignition limit

of scalar dissipation rates is shown in Fig. 9. As the characteristic flow time is reduced to approach the steady ignition limit, the ignition delay becomes more sensitive to the variations in the strain rate.

Many ignition models in turbulent reacting flows are based on the concept that ignition occurs instantaneously when the local scalar dissipation rate at the ignition kernel falls below the steady ignition limit. This is based on the assumption that the flow field variation is sufficiently slower than the ignition delay. However, the result in Fig. 9 suggests that this assumption may not hold, since the ignition delay is a strong function of the flow field *near* the onset of ignition. Further study is needed to resolve this issue.

6. Conclusions

Numerical simulations of one-dimensional unsteady opposed-flow are performed using an adaptive time integration method designed for differential-algebraic systems. The original incompressible boundary layer formulation is modified into a compressible form to alleviate numerical difficulties associated with a high-index system. The numerical method is implemented in the Chemkin software and is capable of dealing with detailed chemical mechanisms and transport properties.

The results for hydrogen/air diffusion flames subjected to oscillatory strain rates demonstrate that the numerical method successfully captures the sinusoidal behavior of the solution. The transient ignition of methane against heated air, which exhibits high temporal stiffness, is also successfully computed. The results show that the ignition delay becomes more sensitive to the strain rate as the flow condition approaches the steady ignition limit.

Acknowledgment

This work has been supported by the US Department of Energy, Office of Basic Energy Sciences, Chemical Sciences Division. The author would like to thank Dr. A. E. Lutz of Sandia National Laboratories and Profs. L. L. Raja and R. J. Kee of Colorado School of Mines for their assistance in the development of the numerical method.

References

Ascher, U. M. and Petzold, L. R., 1998, *Computer Methods for Ordinary Differential Equations and Differential-Algebraic Equations*, SIAM, Philadelphia, PA.

Bilger, R. W., 1988, "The Structure of Turbulent Nonpremixed Flames," *Twenty-Second Symposium (International) on Combustion*, The Combustion Institute, Pittsburgh, PA, pp. 475 ~488.

Brenan, K. E., Campbell, S. L. and Petzold, L. R., 1996, *Numerical Solution of Initial-Value Problems in Differential Algebraic Equations*, 2nd ed., SIAM, Philadelphia, PA.

Frenklach, M., Wang, H., Goldenberg, M., Smith, G. P., Golden, D. M., Bowman, C. T., Hanson, R. K., Gardiner, W. C. and Lissianski, V., 1995, "GRI-Mech — An Optimized Detailed Chemical Reaction Mechanism for Methane Combustion," *GRI Report* No. GRI-95/0058.

Grcar, J. F., 1992, "The Twopnt Program for Boundary Value Problems," *Sandia Report* SAND91-8230.

Im, H. G., Chen, J. H. and Chen, J.-Y., 1999, "Chemical Response of Methane/Air Diffusion

Flames to Unsteady Strain Rate," *Combustion and Flame*, Vol. 118, pp. 204~212.

Kee, R. J., Dixen-Lewis, G., Warnatz, J., Coltrin, M. E. and Miller, J. A., 1986, "A Fortran Computer Code Package for the Evaluation of Gas-Phase Multicomponent Transport Properties," *Sandia Report* SAND86-8246,

Kee, R. J., Miller, J. A., Evans, G. H. and Dixon-Lewis, G., 1988, "A Computational Model of the Structure and Extinction of Strained, Opposed Flow, Premixed Methane-Air Flames," *Twenty-Second Symposium (International) on Combustion*, The Combustion Institute, pp. 1479~1494.

Kee, R. J., Rupley, F. M. and Miller, J. A., 1991, "Chemkin-II : A Fortran Chemical Kinetics Package for the Analysis of Gas-Phase Chemical Kinetics," *Sandia Report* SAND89-8009B.

Lee, S. R., Park, S. S. and Chung, S. H., 1995, "Flame Structure and Thermal NOx Formation in Hydrogen Diffusion Flames with Reduced Mechanisms," *KSME Journal*, Vol. 9, No. 3, pp. 377~384.

Lutz, A. E., Kee, R. J., Grcar, J. F. and Rupley, F. M., 1996, "OPPDIF : A Fortran Program for Computing Opposed-flow Diffusion Flames," *Sandia Report* SAND96-8243.

Petzold, L. R., 1982, "A Description of DASSL : A Differential/Algebraic System Solver," *Sandia Report* SAND82-8637.

Raja, L. L., Kee, R., J. and Petzold, L. R., 1998, "Simulation of the Transient, Compressible, Gas-Dynamic, Behavior of Catalytic-Combustion Ignition in Stagnation Flows," *Twenty-Seventh Symposium (International) on Combustion*, The Combustion Institute, pp. 2249~2257.

Schlichting, H., 1979, *Boundary Layer Theory*, 7th ed., McGraw-Hill, p. 95.

Yetter, R. A., Dryer, F. L. and Rabitz, H., 1991, "A Comprehensive Reaction Mechanism for Carbon Monoxide/Hydrogen/Oxygen Kinetics," *Combust. Sci. Tech.*, Vol. 79, pp. 97~128.